International Symposium
On Turbulence and Shear Flow
Phenomena (TSFP-8)
August 28 - 30, 2013 Poitiers, France

SPANWISE OSCILLATORY WALL MOTION IN CHANNEL FLOW: DRAG-REDUCTION MECHANISMS INFERRED FROM DNS-PREDICTED PHASE-WISE PROPERTY VARIATIONS AT $Re_\tau = 1000$

L. Agostini, E. Touber, M. A. Leschziner
Department of Aeronautics
Imperial College London
South Kensington Campus, London SW7 2AZ, U.K
l.agostini@imperial.ac.uk

ABSTRACT

A DNS-based study is presented, which focuses on the response of near-wall turbulence and skin friction to the imposition of an oscillatory spanwise wall motion in channel flow. The main focus is on transients in the drag, at Re_τ=1000, that are in the form of moderate oscillatory variations in the phase-averaged skin friction and near-wall turbulence around the low-drag state at non-optimal actuation conditions at which the drag reduction margin does not reach the highest possible level. The study reveals a distinctive hysteresis in the periodic fall and rise of the drag, and the results allow the interaction between drag and the turbulence response to the unsteady Stokes strain to be illuminated.

1 Introduction

There are numerous studies in the relevant literature that deal with the effects of spanwise wall oscillation on the streamwise friction drag. Most report DNS results for channel flow at relatively low Reynolds numbers, typically $Re_\tau = O(200-500)$ (e.g. Quadrio & Ricco (2004); Ricco & Quadrio (2008); Touber & Leschziner (2012)). Moreover, the large majority focus on, or confine themselves to, the time-averaged conditions that prevail when the Stokes strain has driven the flow to its final low-drag state, the drag reducing by over 40 % in some cases. In contrast, very few deal with the processes that drive turbulence and drag, upwards or downwards, during unsteady or transient phases following the onset of actuation or as a consequence of Stokes-strain-induced cyclic variations.

Quadrio & Ricco (2003); Xu & Huang (2005*a*) are two examples of studies which have examined the *temporal* evolution of the drag-reduction process in channel flow, following the sudden imposition of spanwise oscillations. These reveal a behaviour that is not observed within the low-drag state. For example, the drag and turbulence intensity were observed to reduce in a non-monotonic fashion, with turbulence production experiencing *overshoots* during the transient path towards the low-drag state, the final level being attained within about three oscillation periods. A recent study by Ricco *et al.* (2012) considers specifically the relationship between enstrophy and dissipation in an effort to illuminate the mechanism driving the flow toward the low-drag state. The authors argue, based on DNS studies of the transient response of the drag at $Re_\tau = 200$ following a sudden start in the actuation, that the key mechanism is an increase in the enstrophy, provoked by the Stokes strain, and hence a rise in the turbulence dissipation, which then causes turbulence and drag to decrease. Whether the paradigm is supported by the present observations is a question that is addressed in the paper as part of an analysis of data derived from direct numerical simulations at $Re_\tau = 1000$ (the bulk Reynolds number being approximately 20000, based on half-channel height), the highest so far published. In contrast to earlier studies, the emphasis is on the periodically time-varying, phase-averaged fields of stochastic properties, with periodicity provoked by actuation at the non-optimal period $T^+ = 200$. The optimum actuation, yielding the highest drag-reduction margin, is at $T^+ \approx 100$. However, at this value, periodic fluctuations are insignificant, which renders this state unsuitable for analysing mechanisms driven by cyclic drag variations.

2 Computational Conditions

The actuation under consideration is restricted to a purely sinusoidal spanwise oscillation of the wall: $W(t) = W_m \sin(2\pi t/T)$ with $W_m{}^+ = W_m/u_\tau = 12$ and $T^+ = T u_\tau{}^2/\nu = 100$ or 200. These values are the same as those used by Touber & Leschziner (2012) at $Re_\tau = 500$ as well as others reporting DNS studies investigating drag-reduction phenomena in channel flow at lower Re_τ values.

All simulations were performed over the same box of length, height and depth $4\pi h \times 2h \times 2\pi h$, respectively, corresponding to approximately $12 \times 2 \times 6 \times 10^3$ wall units. The box was covered by $1056 \times 528 \times 1056 (= 589 \times 10^6)$ nodes. The corresponding cell dimensions were Δx^+, $\Delta y^+{}_{min}$, $\Delta y^+{}_{max}$, $\Delta z^+ = 12.2, 0.4, 7.2, 6.1$. The maximum CFL number was limited to 0.25. In the actuated flows, data were collected over a period $t^+ = 4600$ (about 7 flow-through times), corresponding to 46 and 23 actuation periods at T^+=100 and 200, respectively. The adequacy of the resolution and convergence of phase-averaged quantities were investigated in various ways, including a simulation of the unactuated flow over a grid of 1200 M cells, an examination of the resolved dissipation, relative to the imbalance of other terms in the turbulence-energy budget, an

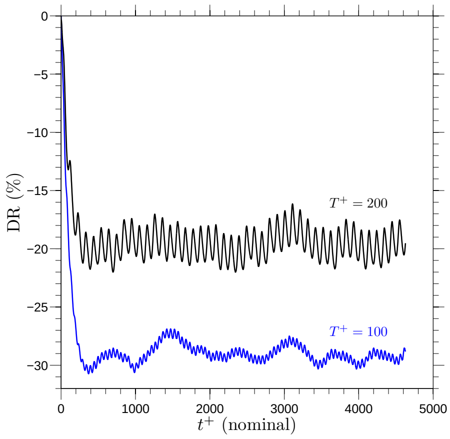

(a)

Figure 1. (a) temporal variations of the wall-integrated skin-friction reduction

evaluation of the ratio of cell distances to the Kolmogorov length scale and integration over different subsets of actuation cycles.

3 Results

Fig.1 shows the temporal variations of skin-friction reduction for $T^+ = 100$ and 200, starting from the converged state of the unactuated baseline flow. The respective time-averaged drag-reduction margins are 29% and 21%, relative to 32% and 25% at $Re_\tau = 500$ (Touber & Leschziner (2012)). The temporal distributions confirm the statement made earlier that the low-drag state is reached after around 3 actuation cycles. This has also been observed earlier – for example, by Xu & Huang (2005*b*). Irrespective of actuation-provoked oscillations, only significant at $T^+ = 200$, the drag displays long-time-scale fluctuations, and these identify the *footprinting* by energetic outer structures (super-streaks), as discussed by Marusic *et al.* (2010).

To obtain some of the results to follow, the large-scale oscillations were removed from the C_f signal by applying the *Hilbert-Huang Transform* to the data in Fig.1, after which the nearly pure oscillatory signal was averaged over all actuation cycles, to yield the cycle-representative distribution shown in Fig.2.

This figure juxtaposes phase-space contour plots of the phase-wise *derivative* of the Stokes strain and the streamwise stress and its production with the cycle-representative C_f variation. The focus on the Stokes-strain *derivative* is motivated by Touber & Leschziner's observation that rapid phase-wise changes in the direction of the strain vector - equivalent to rapid changes in the Stokes strain – tend to disrupt the organisation and structure of the streaks, while low rates (referred to below as 'lingering') tends to favour the re-establishment of the streaks in the direction of the strain vector. It is noted first that the skin-friction variation is *not* sinusoidal, i.e. does not follow faithfully the actuation. Most prominently, the phase over which C_f declines is longer than that over which it recovers. This difference is quantified in Fig.3. Plot (a) contains three curves: the phase-averaged C_f and two purely sinusoidal variations, the periods of which match, respectively, the lowest and the highest phase rates of change in C_f (i.e. the locally lowest and highest frequencies). Plot (b) shows the phase-wise

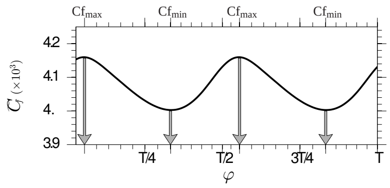

(a)

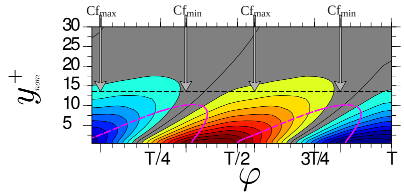

(b)

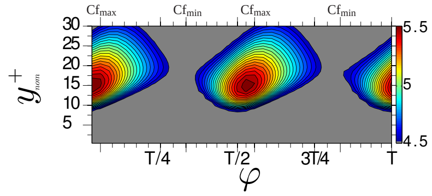

(c)

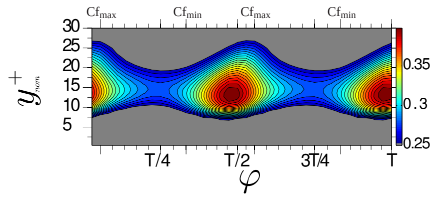

(d)

Figure 2. Correlation between (a) phase-wise skin-friction fluctuations, (b) the phase-wise derivative of the Stokes strain (dashed magenta curve is the locus of equal Stokes strain and streamwise strain), (c) the streamwise Reynolds stress and (d) the production of the streamwise Reynolds stress, all at $T^+ = 200$.

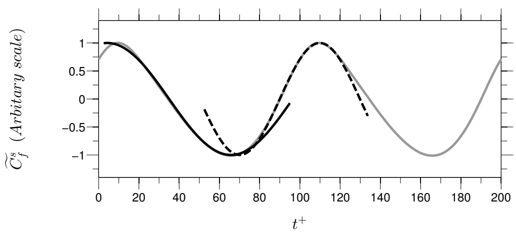

(a)

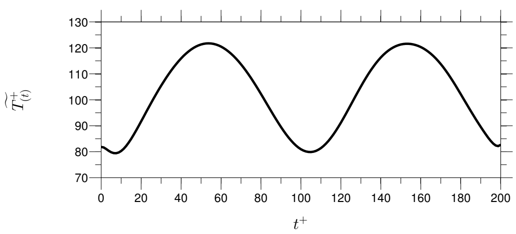

(b)

Figure 3. (a) Phase-averaged skin-friction variation and sinusoidal signals having the maximum and minimum periods of C_f, (b) phase-wise variation of period of sinusoidal signal representing C_f locally.

variation of the 'instantaneous' period of a sinusoidal signal which is the best fit to the local behaviour of C_f. The two sinusoidal signals in plot (a) have periods corresponding to the peak and trough of the distribution in plot (b). This shows that the equivalent wall-scaled period of the sinusoidal signal varies between 78 and 122, relative to the nominal value $T^+/2 = 100$. Next, Fig.2 shows that minima and maxima in the streamwise stress and its production at $y^+ \approx 13-15$ are well correlated with corresponding skin-friction minima and maxima, with the production leading the stress by a small phase margin. To accentuate the relationship between the skin friction and the Stokes strain, arrows have been inserted in the relevant plots, which link skin-friction minima and maxima and to particular regions of the Stokes-strain *derivative* at $y^+ = 13.5$. This juxtaposition highlights the fact that the skin-friction-reduction phase coincides with high level of phase-wise changes in the Stokes strain. In contrast, phases of increasing skin friction coincide with 'lingering' and high Stokes strain. The comparison between the skin friction and the Stokes strain, at the wall-distance at which the streaks are strongest, suggests the presence of a lag between maximum Stokes strain and maximum skin friction, on the one hand, and minimum Strokes strain and minimum skin friction, on the other. This lag is around $0.1-0.15T$, corresponding to t^+=20-30, a figure that accords with that observed by Touber & Leschziner (2012) who show that the phase-dependent *switch* in streak direction lags behind the change in strain-direction at $y^+ \approx 12$ by about $0.15T^+$. This comparison thus appears, prima facie, to provide support for earlier observations that high rates of change in the Stokes strain in the upper part of the viscous sublayer cause a disruption in the streaks and the mechanism sustaining them, while low rates of change promote a re-generation of the streaks. When C_f and the turbulent stresses reach their respective maximum values, almost simultaneously, the streaks are at their strongest and assume an orientation that corresponds broadly to that of the strain vector at the nominal streak location. This is illustrated in Fig.4 (a) and (c), in which the line contours identify the footprints of large-scale outer structures, determined from the two leading modes of the Hilbert-Huang Transform.

In what follows it will be argued that the above interactions, while not invalid, are too restrictive, in so far as the response of turbulence to the oscillatory forcing is also linked to a different type of interactions very close to the wall, and a diffusive cross-flow propagation of perturbations. To illuminate the pertinent processes, consideration is given to the phase-wise changes in various turbulence quantities across the near-wall layer. First, Fig. 5 shows the profiles of the phase-averaged shear stress at different phase positions during the actuation cycle. Fig.5(a) relates to the period in which the drag (C_f) decreases from its maximum to its minimum, while Fig.5(b) pertains to the following drag-rise period. During the reduction phase, the shear stress within the viscous sublayer drops progressively and uniformly within $y^+ \approx 30$, with the maximum stress shifting outwards by about 30 wall units. In the drag-rise phase, the shear stress increases again, but it is remarkable that this increase is far from following a same path as the preceding decrease – i.e. the cyclic process is hysteretic. Thus, the rise in the shear-stress occurs preferentially in the lower parts of the viscous sublayer, with a rapid rise close to the wall propagating outwards across the viscous sublayer, the maximum at around $y^+ \approx 25$ being re-established much more quickly than it had been eroded in the preceding drag-decline phase.

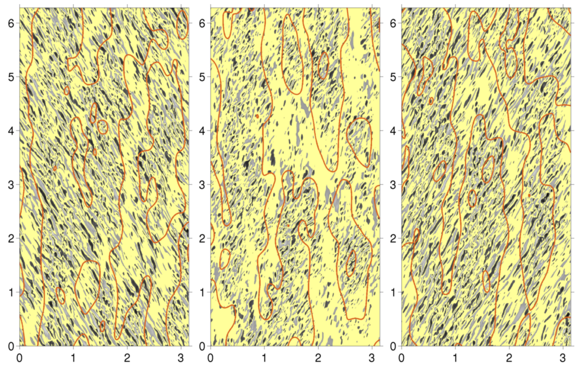

(a) (b) (c)

Figure 4. Streaky near-wall structure at $y^+ = 13.5$, identified by streamwise-velocity fluctuations; (a) at maximum C_f and negative Stokes strain; (b) at minimum C_f; at (c) maximum C_f and positive Stokes strain. Red contours identify large-scale motions (first two Hilbert-Huang modes), small-scale velocity fluctuations (modes 3 and higher) are excluded below a magnitude of 7% of the maximum value of the rms fluctuations.

The above *hysteresis* is brought out well in Fig.6, which shows phase-wise contour plots of fluctuations in the shear and wall-normal stresses, $(\widetilde{u''v''}^+ - \overline{u''v''}^+)$ and $(\widetilde{v''v''}^+ - \overline{v''v''}^+)$, respectively. The dashed contour lines in the plots indicate, respectively, 75%, 50%, 25% and 0% of the maximum Stokes strain. Both plots show that the decline in the *magnitude* of the stresses within the viscous sublayer progresses over a longer portion of the period than the increase. Moreover, the patterns of decline and rise in the stresses close to the wall differ substantially, an issue discussed further below.

One striking feature in Fig.6 is the forward tilt of the contours, suggesting a 'wave'-like propagation of disturbances along a characteristic direction in the space-time domain, which both plots represent. The angle of inclination of the contours (different from the shallower orientation of the lines of zero and maximum Stokes strain) implies that the 'speed' of propagation is close to u_τ, which is consistent with the supposition that the propagation is associated with viscous diffusion. A second feature seen in the contour maps is that, consistent with differences observed in Fig. 5, the increase in the shear stress and the wall-normal stress, the latter governing the production of the former, tends to occur preferentially in the lower part of the viscous sublayer, while the decline occurs predominantly further away from the wall.

An apparent contraction to the previously proposed causal relationship between stresses and the time-rate-of-change in the Stokes strain at $y^+ \approx 13$ (Fig.2) is that the decline and rise in the stresses close to the wall appear to be well correlated with the *magnitude* of the Stokes strain, not its *rate of change*. Thus, a high level of Stokes strain provokes a decline in the stresses, while a low level is accompanied by an increase in the stresses. However, this correlation only applies to the region close to wall, but not to the upper part of the viscous sublayer. Here, a flow property that appears to play an important role is the *skewness*, given in Fig. 7. This is characterised by the wall-normal gradient of the velocity-vector orientation θ, i.e. $\partial\theta/\partial y$. The figure shows colour contours of the skewness gradient, and a black con-

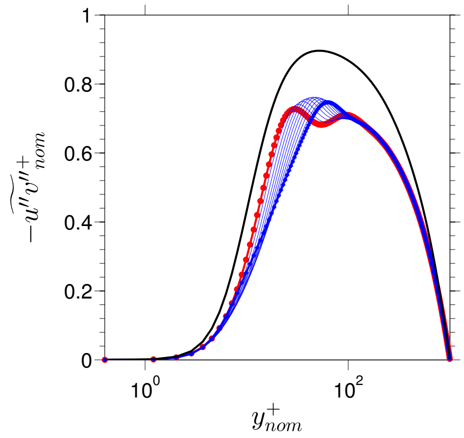

(a)

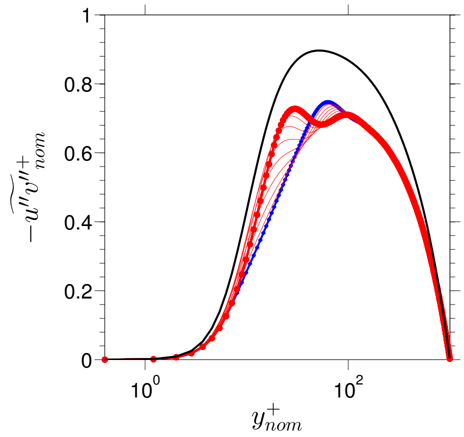

(b)

Figure 5. Phase-wise variations of profiles of the shear stress during (a) the drag-reduction phase and (b) the drag-increase phase, at $T^+ = 200$. Thick (red) line with solid circles corresponds to the maximum skin-friction phase value; thick (blue) line with crosses corresponds to minimum skin-friction phase value.

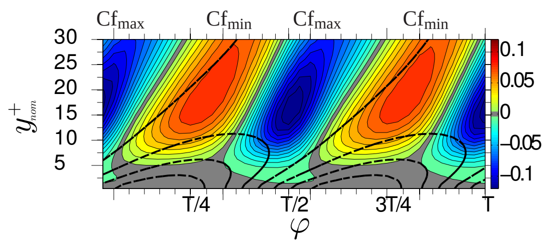

(a)

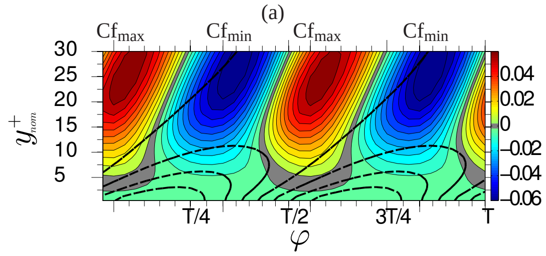

(b)

Figure 6. Phase-wise variations of the fluctuations (a) in the shear-stress $(\widetilde{u''v''}^+ - \overline{u''v''}^+)$ and (b) in the wall-normal stress $(\widetilde{v''v''}^+ - \overline{vv}^+)$. Dashed contours represent loci of 75%, 50%, 25% and 0% Stokes strain.

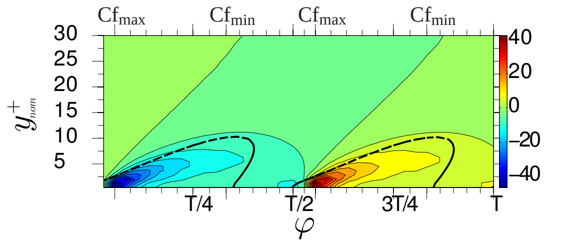

Figure 7. Skewness map (wall-normal derivative of velocity angle). The black dashed curves are loci of equal streamwise and Stokes strains, with regions below the curves characterised by high Stokes strain.

tour line that represents the locus $\partial \widetilde{W}/\partial y = \partial \widetilde{U}/\partial y$. The skewness is observed to be very high in lower regions of the viscous sublayer and within the domain in which the Stokes strain is also high. However, contours of high skewness are strongly inclined, and skewness is low in the upper portion of the viscous sublayer, thus unlikely to greatly influence *directly* the decay and increase in streak strength at $y^+ \approx 12-15$. Skewness near the wall is especially high following the phase value at which the skin friction peaks (the $C_{f,max}$ locations), following which the decline in turbulence quantities commences close to the wall and is pronounced in regions in which turbulence activity is depressed. It thus seems that high skewness is instrumental in causing a decline in the streak-regeneration process that is initiated in the lower part to the viscous sublayer. In contrast, when skewness is relatively low, around and beyond the location of $C_{f,min}$, the streak regeneration process can re-establish; this is compatible with the phase-wise behaviour of the stresses in Fig. 6.

A partial interpretation of the mechanisms leading to the hysteresis, exemplified by Fig. 6, rests on the proposal of a two-stage cyclic process. In the first, the Stokes strain and high skewness depress the turbulence activity within the lower part of the viscous layer (see especially Fig.6(b)), with strong near-wall damping propagating outwards into higher reaches of the sublayer. Structurally, this may be equated with a disruption of the regeneration of new streaks, possibly in conjunction with (old) and weakening streaks being 'lifted' upwards, away from the viscous sublayer. Second, as the phase progresses, the decrease in Stokes strain and skewness, and the recovery of the dominance of the streamwise strain, promote the creation of new streaks close to the wall, by shear-stress and streamwise-normal-stress production, with turbulence propagating into the upper region of the viscous sublayer. Alongside this diffusive process, total-strain-induced turbulence generation in the upper part, coinciding with relatively low skewness, promotes the increase in turbulence activity, thus giving rise to maxima at the wall-normal location around which the streaks are strongest and most pronounced. The above argument on the decay and lift-up of 'old' streaks and the regeneration of new ones at the wall will be revisited later by reference to enstrophy fields. This interpretation leads to the conclusion that the earlier focus on the link between variations in the Stokes strain at $y^+ = 12-15$ and the streak-decay/re-generation process is only one part of a more complex interaction scenario.

Fig.8 shows phase-wise variations of the budgets for the streamwise and the shear stress components. Two sets of plots are presented: the left-hand side plot in each set relates

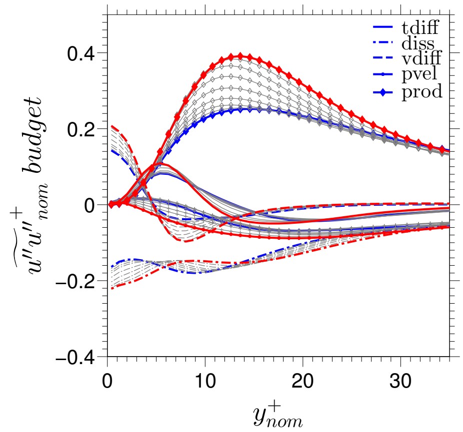

(a)

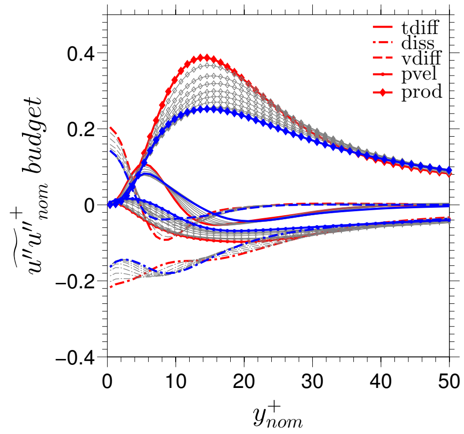

(b)

Figure 8. Phase-wise fluctuations of the budget contributions for the streamwise normal stress during (a) the drag-increase phase and (b) the drag-decrease phase. Thick (red) lines with solid circles corresponds to the maximum skin-friction phase value; thick (blue) lines with crosses corresponds to minimum skin-friction phase value.

to the drag-rise phase, while the right-hand side one relates to the drag-decrease phase, the phase values at which C_f reaches its maximum and minimum being indicated by the thicker solid lines with symbols. The time-rate-of-change contributions are very small and thus omitted. The hysteresis is especially pronounced in the production term, which is seen to vary substantially despite the rather modest oscillations in skin friction. During the drag reduction phase, the reduction in the production occurs, again, uniformly across the whole viscous sublayer, with the peak gradually reducing, without shifting significantly its wall-normal location. In contrast, in the drag-increase phase, there is, as before, a preferential increase in production in the lower parts of the viscous sublayer, followed by a delayed increase in the upper part. An important point to highlight in the $\widetilde{u''u''}^+$ budget is that the substantial fluctuations in production, reflecting variations in the streak strength, are balanced mainly by corresponding fluctuations in diffusion and pressure-velocity interaction. In contrast, variations in the dissipation level are small. Morever, during the drag-reduction phase, the dissipation decreases over almost the entire wall-normal extent, with the reverse occuring during the drag-increase phase. As the dissipation of the streamwise stress dominates the turbulence-energy dissipation, the

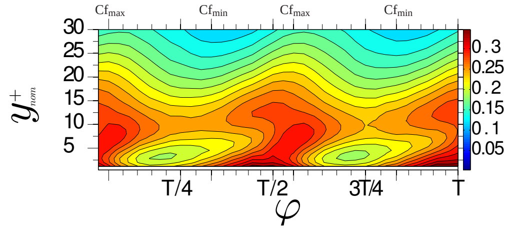

(a)

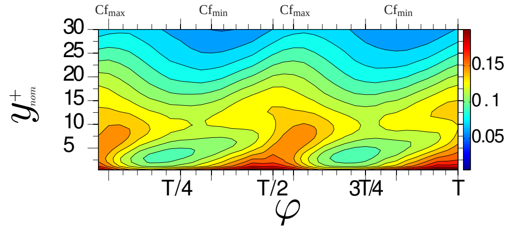

(b)

Figure 9. Phase variation of : (a) turbulence-energy dissipation ε_{ii}, (b) enstrophy $2\widetilde{\omega_i''\omega_i''}$.

expectation is that drag reduction and increase go hand-in-hand with a (modest) decline and increase in dissipation, respectively. This observation contradicts the mechanism proposed by Ricco *et al*. (2012), which is based on the argument that the enstrophy is enhanced by the Stokes motion, and thus the increase in enstrophy and dissipation are held responsible for the drag reduction. This contradiction will be reinforced by results for the enstrophy discussed below.

Fig.9 compares phase-wise variations of the enstrophy and of the dissipation of turbulence energy. Entirely in accord with expectations, the two are found to be closely correlated. Importantly, both decline during the phase in which the drag decreases, and rise when the drag increases. Next, Fig.10 shows phase-wise profiles of the enstrophy component, $\widetilde{\omega_y''\omega_y''}$. This component is being given preference, because it reflects the significant phase-dependent variations in streak strength and structure during the actuation cycle – although the increase in spanwise fluctuations, due to Stokes-strain-induced production, also contributes, albeit modestly, to the observed phase sensitivity. Consistent with properties already presented, the enstrophy also shows a distinctive hysteresis. Starting from the highest variation, corresponding to the skin-friction peak in Fig.2, the enstrophy decreases uniformly over the viscous sublayer, with the peak reducing and shifting away from the wall, from $y^+ \approx 13$ towards $y^+ \approx 25$. As the drag increases again, there is a rapid increase, over a period of around $t^+ \simeq 50$, in the enstrophy in the lower parts of the viscous sublayer, with peak rapidly shifting towards the wall and the enstrophy rising more slowly in the outer portion of the sublayer. Hence, in accord with comments made earlier in relation to Fig.6, the implication is, again, that the decay of the streaks is broadly uniform across the viscous sublayer and that 'old' streaks are being lifted away from the wall, while the regeneration of new streaks is initiated much closer to the wall.

Phase-space contour maps for the streamwise and wall-normal components of the enstrophy and their respective productions are shown in Fig.11. A first observation derived from Fig.11 is that the enstrophy-production rates are well correlated with the respective enstrophy components themselves. Second, the streamwise component drops during the drag-reduction phase, while it rises when the drag increases.

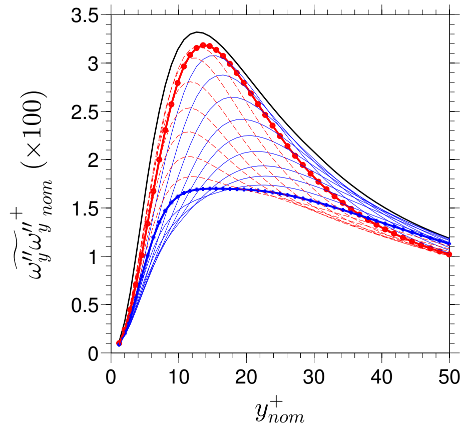

(a)

Figure 10. Phase-wise variations of the wall-normal component of the enstrophy at T^+ =200. Thick (red) line with solid circles corresponds to the maximum skin-friction phase value; thick (blue) line with crosses corresponds to minimum skin-friction phase value; solid black line relates to the unactuated flow.

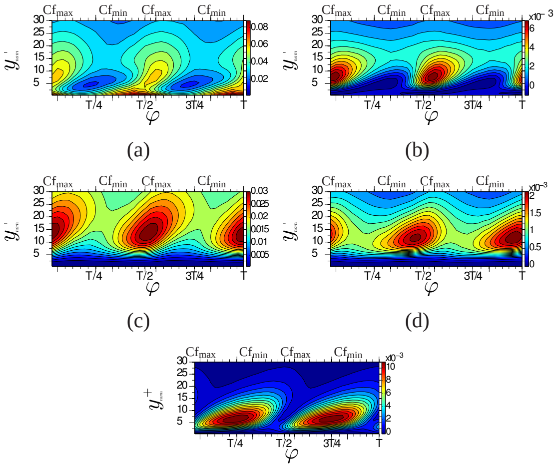

(a) (b)

(c) (d)

(e)

Figure 11. Phase variations of the enstrophy components (left colums) and their production rates (right colums): (a) and (b) x-component;(c) and (d) y-component.

This accords with expectations, as the phases of low streamwise enstrophy go hand-in-hand with low wall-normal motions and hence wall-normal mixing of streamwise momentum. Third, consistent with low and high streamwise enstrophy are correspondingly low and high wall-normal enstrophy levels $\widetilde{\omega_y''\omega_y''}$. As noted earlier, this component is indicative of the decay, lift-off and regeneration of the streaks during the actuation period. The fact that the enstrophy levels are relatively low (though fluctuating strongly) is due to the substantial spanwise distances, of order 100 wall units, separating the streak. Here too, the rise and fall of both production and enstrophy are well correlated.

4 Conclusions

The present results display features that are, prima facie, compatible with the drag-reduction scenario proposed by Touber & Leschziner (2012) - namely, that that phase intervals of skin-friction increase are associated with high and slowly varying Stokes strain at the level at which the streaks reside, while phase intervals of skin-friction decline are associated with rapidly varying, low Stokes strain at the same level. However, if attention is focused on the region very close to the wall, a more complex scenario emerges.

In *lower* parts of the viscous sublayer, the phase-wise rise and decline in turbulent stresses and associated turbulence properties are driven not only by the magnitude of and rate of change in the Stokes strain itself, but also the skewness. Thus, the observed collocation of the turbulence rise and decline with, respectively, regions of low and high Stokes strain – rather than the reverse – is caused by the influence of the near-wall skewness which tends to disrupt the streak-generation process over and above that caused by the rapid phase-wise rate or change of the Stokes strain. This complements the paradigm that links the skin friction and streaks strength only to the *the rate of change* of the Stokes strain in upper parts of the viscous sublayer. The different interactions during the drag-increase and the drag-decrease phases are one source for the observed drag hysteresis.

The phase-averaged budgets for the streamwise normal stress and the shear stress show that fluctuations in the production are substantial and are counteracted mainly by diffusion and pressure-velocity interaction. Importantly, fluctuations in dissipation are not only minor, but fluctuate broadly in harmony with skin-friction variations: the dissipation declines when the skin-friction declines and vice-versa.

Enstrophy and dissipation are closely correlated: both decline in phase intervals in which the skin-friction declines and vice-versa. This observation, and the previous conclusion, do not support the drag-reduction scenario advanced by Ricco *et al.* (2012). Drag fluctuations are primarily driven by production fluctuations, with other terms following suit to satisfy the budget constraints.

ACKNOWLEDGMENT

The authors acknowledge the financial support provided by the UK academic funding agency EPSRC, through grant EP/G061556/1, EADS UK Limited and Airbus Operations Limited. The simulations were performed on the UK's National HPC facility HECToR, as part of the aforementioned EPSRC grant and with additional resources provided by the EPSRC-funded UK Turbulence Consortium.

REFERENCES

Marusic, I., Mathis, R. & Hutchins, N. 2010 *Science* **329** (5988), 193–196.

Quadrio, M & Ricco, P 2003 *Journal of Turbulence* (4).

Quadrio, M. & Ricco, P. 2004 *Journal of Fluid Mechanics* **521**, 251–271.

Ricco, P., Ottonelli, C., Hasegawa, Y. & Quadrio, M. 2012 *Journal of Fluid Mechanics* **700** (1), 1–28.

Ricco, P. & Quadrio, M. 2008 *International Journal of Heat and Fluid Flow* **29** (4), 891–902.

Touber, E. & Leschziner, M. A. 2012 *Journal of Fluid Mechanics* **693**, 150–200.

Xu, Chun-Xiao & Huang, Wei-Xi 2005*a* *Physics of Fluids* **17**, 018101.

Xu, C. X. & Huang, W. X. 2005*b* *Physics of Fluids* **17**, 018101.